–Electronic Supporting Information–
Effect of Exchange-Correlation Functionals on the Estimation of Migration Barriers in Battery Materials

Reshma Devi[1], Baltej Singh[2], Pieremanuele Canepa[2,3,+], and Gopalakrishnan Sai Gautam[1,*]

[1]Department of Materials Engineering, Indian Institute of Science, Bengaluru 560012, Karnataka, India
[2]Department of Materials Science and Engineering, National University of Singapore, Engineering Drive, 117575, Singapore
[3]Department of Chemical and Biomolecular Engineering, National University of Singapore, Engineering Drive, 117575, Singapore
[+]pcanepa@nus.edu.sg
[*]saigautamg@iisc.ac.in

S1 Convergence difficulties in nudged elastic band calculations

We faced significant convergence difficulties while performing nudged elastic band (NEB) calculations with regular density functional theory (DFT) and Hubbard U corrected DFT (i.e., DFT+U) frameworks in $LiFePO_4$, NaV_2O_4, $MgMn_2O_4$, and $LiCoO_2$ systems. To tackle the same, we employed one of the following three strategies, *i*) restart the NEB calculation from the previous geometry, if it hits wall time, *ii*) increase the NEB force convergence or energy convergence threshold (usually from |0.05| to |0.07| eV per Å and 0.01 meV to 0.05 meV respectively), or *iii*) if the NEB doesn't converge after multiple attempts of steps *i* and *ii*, obtain the minimum energy pathways (MEPs) and the corresponding migration barriers (E_m) via a single self-consistent-field (SCF) calculation from previously converged NEBs using other functionals. Note that an NEB restart corresponds to re-initializing the NEB, with the last available geometry, after a given NEB calculation has hit the wall time.

For $LiFePO_4$ (Supplementary Figure 3), both GGA-NEB and SCAN-NEB did not converge despite 6-7 restarts and we obtained the corresponding E_m from GGA+U and SCAN+U relaxed NEBs, respectively (via single SCF calculations). While GGA+U-NEB for NaV_2O_4 (Supplementary Figure 8) converged after two restarts, SCAN+U, was not close to convergence even after 7 restarts. Hence, we obtained the SCAN+U E_m for NaV_2O_4 from the corresponding converged geometries of SCAN-NEB. We increased the energy convergence threshold (to 0.05 meV) to converge the SCAN-NEB calculation in $MgMn_2O_4$ after five restarts, while the monovacancy hop of $LiCoO_2$ with SCAN+U took nine restarts to converge. In the case of divacancy hop in $LiCoO_2$, SCAN+U MEPs and E_m were obtained from SCAN-NEB as it did not converge even after 12 restarts.

S2 Calculation of computational time

With respect to estimating the computational time requirement for systems where we relied on single-SCF calculations, we simply added the maximum time taken for a single-SCF calculation, among the converged images, to the total time for convergence that the previous NEB calculation took. For example in the case of $LiFePO_4$ GGA-NEB, we added the maximum time taken among the 9 images during the GGA-SCF to the total time (including restarts) that was taken by the GGA+U NEB to converge. Thus, the computational time per image for the GGA-NEB can be given by the following equation,

$$\text{Computational time per image} = \frac{(\text{Time taken for GGA+}U\text{ NEB per image}) + (\text{Maximum time taken for a single SCF calculation})}{(\text{Number of cores used per image})}$$

Composition	Supercell size	Number of atoms
Layered $LiCoO_2$ (divacancy hop) ($R\bar{3}mH$)	3×3×2	71
Spinel-$LiMn_2O_4$ ($Fd\bar{3}m$)	1×1×1	55
Olivine-$LiFePO_4$ ($Pnma$)	1×2×2	111
Post-spinel-NaV_2O_4 ($Pnma$)	1×4×1	111
Spinel-$MgMn_2O_4$ ($I41/amd$)	2×2×1 (except GGA) 1×1×1 (GGA)	111 (except GGA) 55 (GGA)
Spinel-$Mg_xTi_2S_4$ ($Fd\bar{3}m$)	1×1×1	49
Spinel-$MgSc_2Se_4$ $Fd\bar{3}m$	1×1×1	55
Tetragonal-Na_3PS_4 ($P\bar{4}2_1c$)	2×2×2	127
Orthorhombic-Li_3PO_4 ($Pnma$)	1×2×2	126

Supplementary Table 1. Supercell sizes and number of atoms per image used in the NEB calculations.

Composition	Experimental technique	Measurement range	Synthesis	Ref.
		Electrodes		
Layered-$LiCoO_2$ ($R\bar{3}mH$) (divacancy hop)	Cariable temperature solid-state nuclear magnetic resonance (VT-SS-NMR)	Temperature: 4 K−630 K, diffusion coefficient of 10^{-14} cm^2/s at 400 K gives an activation barrier of 0.3 eV	Stoichiometric powders of Li_2Co_3 and Co_3O_4 were ground, pelletized, and heated at 950°C in air to obtain polycrystalline $LiCoO_2$	1
Spinel-$LiMn_2O_4$ ($Fd\bar{3}m$)	Rotor-synchronized 2D exchange NMR	Temperature:285 K−400 K, Activation Barrier: 0.5±0.1 eV	A single phase $Li[Mn_{1.96}Li_{0.04}]O_4$ compound was investigated for the mobility study	2
Olivine-$LiFePO_4$ (*Pnma*)	Electrochemical Impedance Spectroscopy (EIS)	Temperature: 273 K−313 K, activation barrier: 0.66 eV corresponding to an area specific resistance of 207.6 Ωcm^2 at 25°C	Cathode was prepared by creating a 1-methyl-2-pyrrolidinone based slurry from carbon coated $LiFePO_4$ powder, carbon black, and a polymeric binder in the weight ratio 70:24:6. As-prepared slurry was coated on an aluminium foil and vacuum dried at 80 °C followed by tempering at 120°C for 180 minutes to obtain the electrode	3
Post-spinel-NaV_2O_4 (*Pnma*)	Muon Spin Relaxation (μSR)	Temperature: 10 K−500 K, activation barrier: 0.25 eV	2 grams of polycrystalline NaV_2O_4 sample was prepared from solid state reaction of $Na_4V_2O_7$ and V_2O_3 powders. As-prepared sample was pressed into a disc of 24 mm diameter and 1.5 mm thickness	4
Spinel-$MgMn_2O_4$	μSR	Temperature: 250 K−400 K, activation barrier of 0.7 eV (±0.1ev)	Sol-gel synthesis route involving stoichiometric ratios of metal acetate and deionized water	5
Spinel-$Mg_xTi_2S_4$ ($Fd\bar{3}m$)	Galvanostatic Intermittent Titration Technique (GITT)	Diffusion coefficients obtained for cubic-Ti_2S_4 at 60°C correspond to a barrier of 0.5 eV for x=0.148 in $Mg_xTi_2S_4$	Cubic-Ti_2S_4 cathode in the coin cell was obtained by chemical oxidation of Cu^+ from $CuTi_2S_4$. Mg negative electrode and all-phenyl complex(APC) electrolyte was used to intercalate Mg in to C-Ti_2S_4	6
		Electrolytes		
Spinel-$MgSc_2Se_4$ $Fd\bar{3}m$	VT-SS-NMR	Temperature: 300−400 K, activation barrier: 0.37±0.9 eV	Ball-milled mixture of Mg, Sc, and Se powders were pelletized and secured in steel tubes and subsequently kept in a furnace heated to 1000°C in 1 hour and held at 1000°C for 12 hours to facilitate the solid-state reaction	7
Tetragonal-Na_3PS_4 ($P\bar{4}2_1c$)	EIS	Temperature: 298.5 K−333 K, activation barrier: 0.35 eV	Cold pressed pellets of powdered tetragonal-Na_3PS_4 prepared from mechanochemical milled Na_2S, CaS, and P_2S_5 at 500 rpm for 3–5 hours followed by heat treatment at 700°C	8
Orthorhombic-Li_3PO_4 (*Pnma*)	SS-NMR	Temperature: 200 K−500 K, activation barrier: 0.286±0.6 eV for 80 mol% of Li_3PO_4	Solid solution of $Li_{3+x}P_{1-x}Si_xO_4$ ($0<x<0.4$) was obtained by reacting stoichiometric mixtures of lithium orthosilicate (obtained by firing reagent-grade Li_2CO_3 and amorphous-SiO_2) and γ_{II}-Li_3PO_4 at 1150°C for 6 hours	9

Supplementary Table 2. Experimental techniques used for synthesis and measurement of E_m of the materials considered.

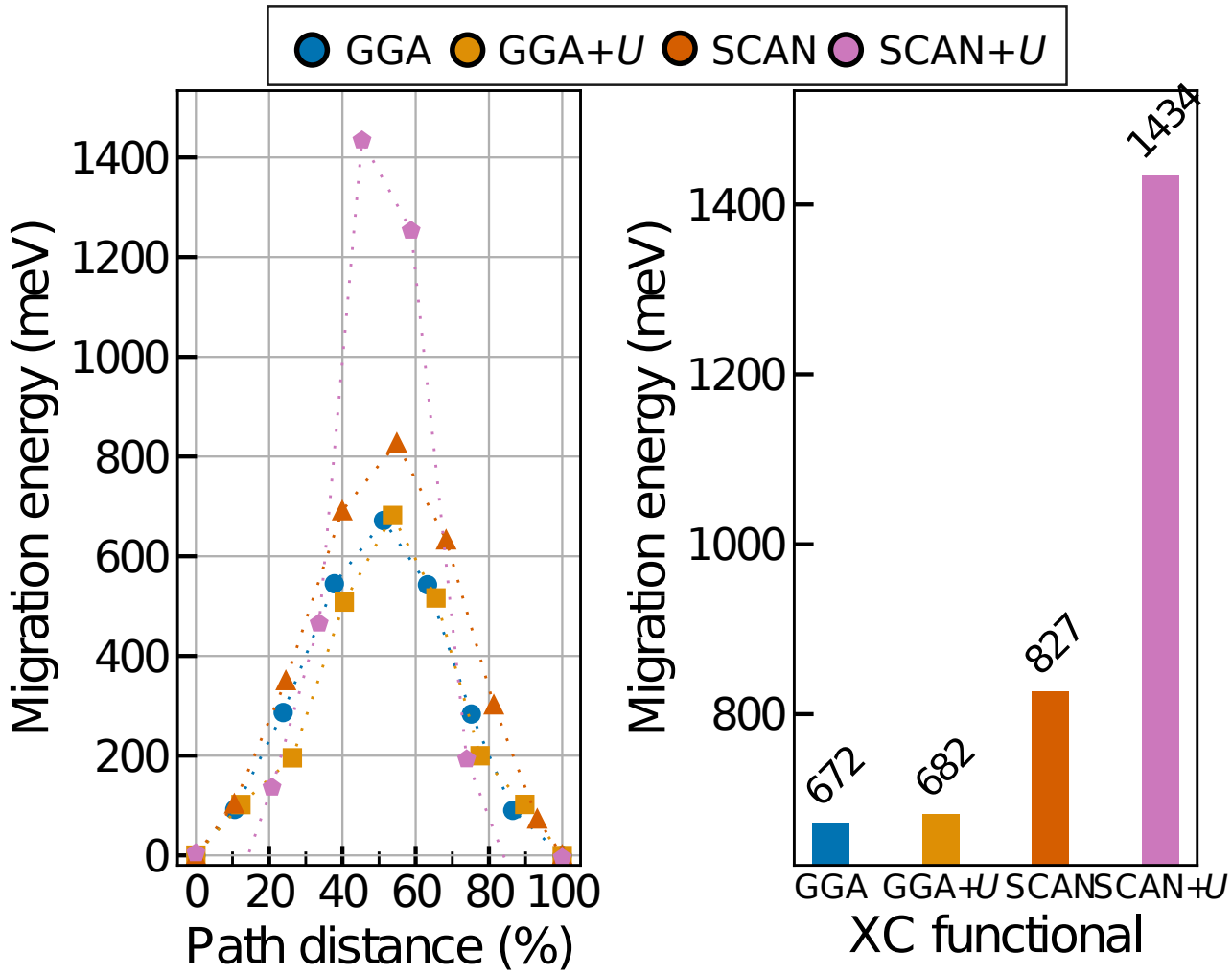

Supplementary Figure 1. MEPs and associated E_m for $LiCoO_2$ for the oxygen dumbbell hop, or the monovacancy mechanism, as calculated using GGA, GGA+*U*, SCAN, and SCAN+*U*.

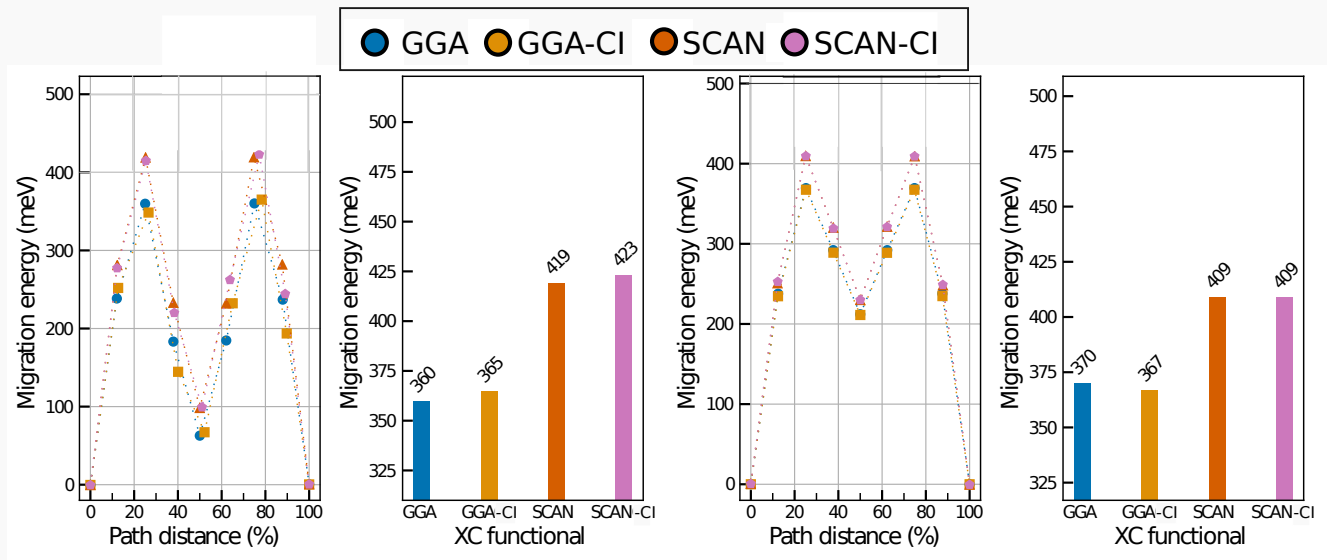

Supplementary Figure 2. MEPs and E_m for $MgSc_2Se_4$ without and with the inclusion of uniform background charge (NELECT). CI in the figure panels corresponds to climbing image.

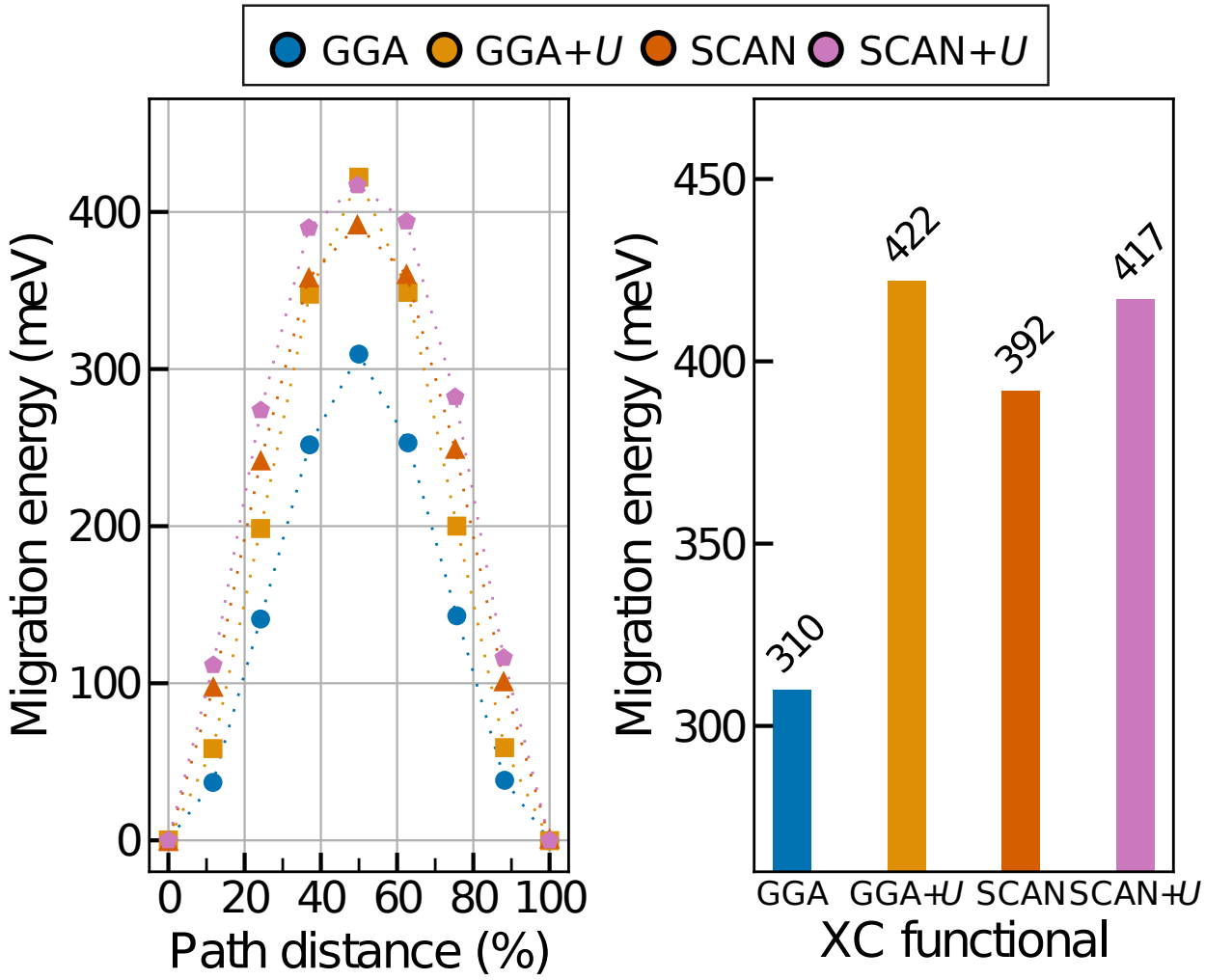

Supplementary Figure 3. MEPs and E_m for $LiFePO_4$. The GGA and SCAN barriers were obtained from single-SCF calculations based on converged GGA+*U*-NEB and SCAN+*U*-NEB geometries, respectively.

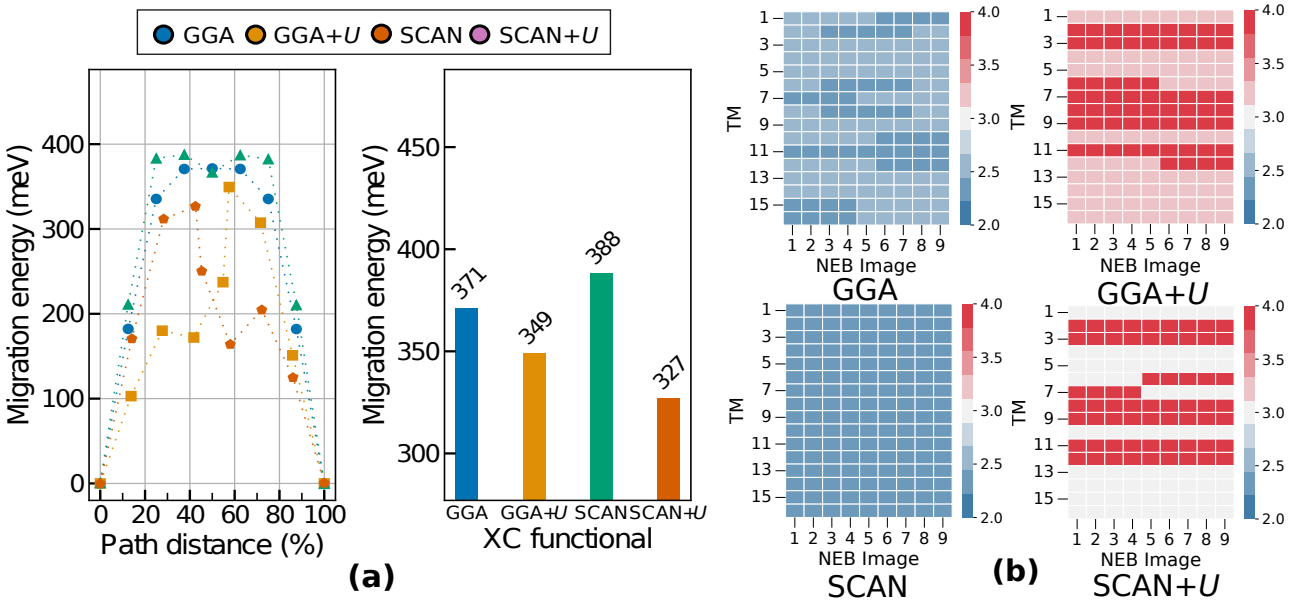

Supplementary Figure 4. MEPs and E_m for $LiMn_2O_4$, along with the on-site magnetic moments of all transition metal (TM) ions.

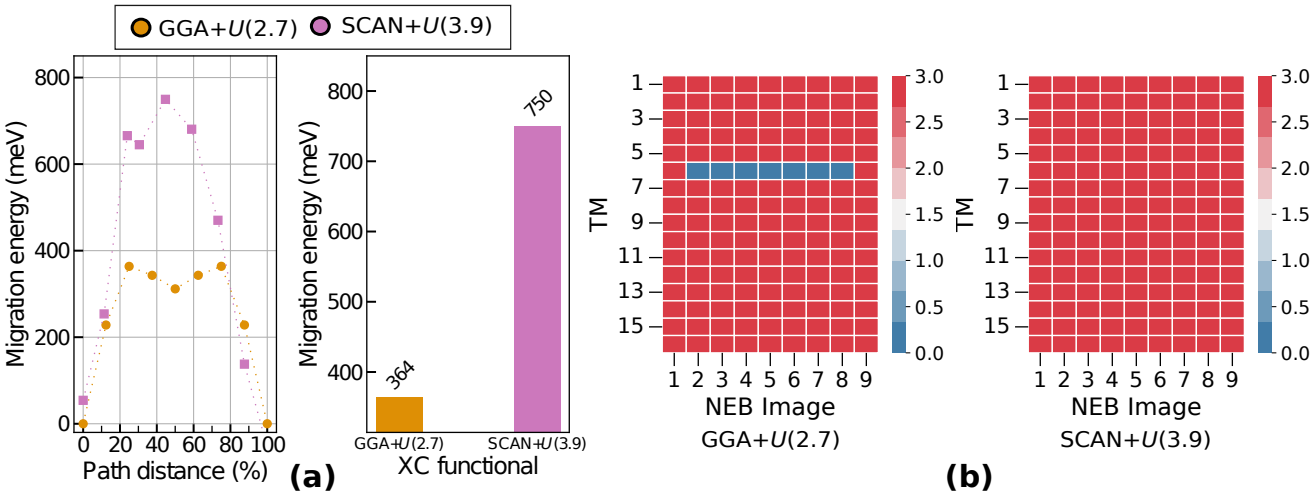

Supplementary Figure 5. MEPs and E_m for $LiMn_2O_4$, calulated for GGA+U and SCAN+U with U values 2.7 and 3.9 repectively. Panel b shows the corresponding magnetic moments

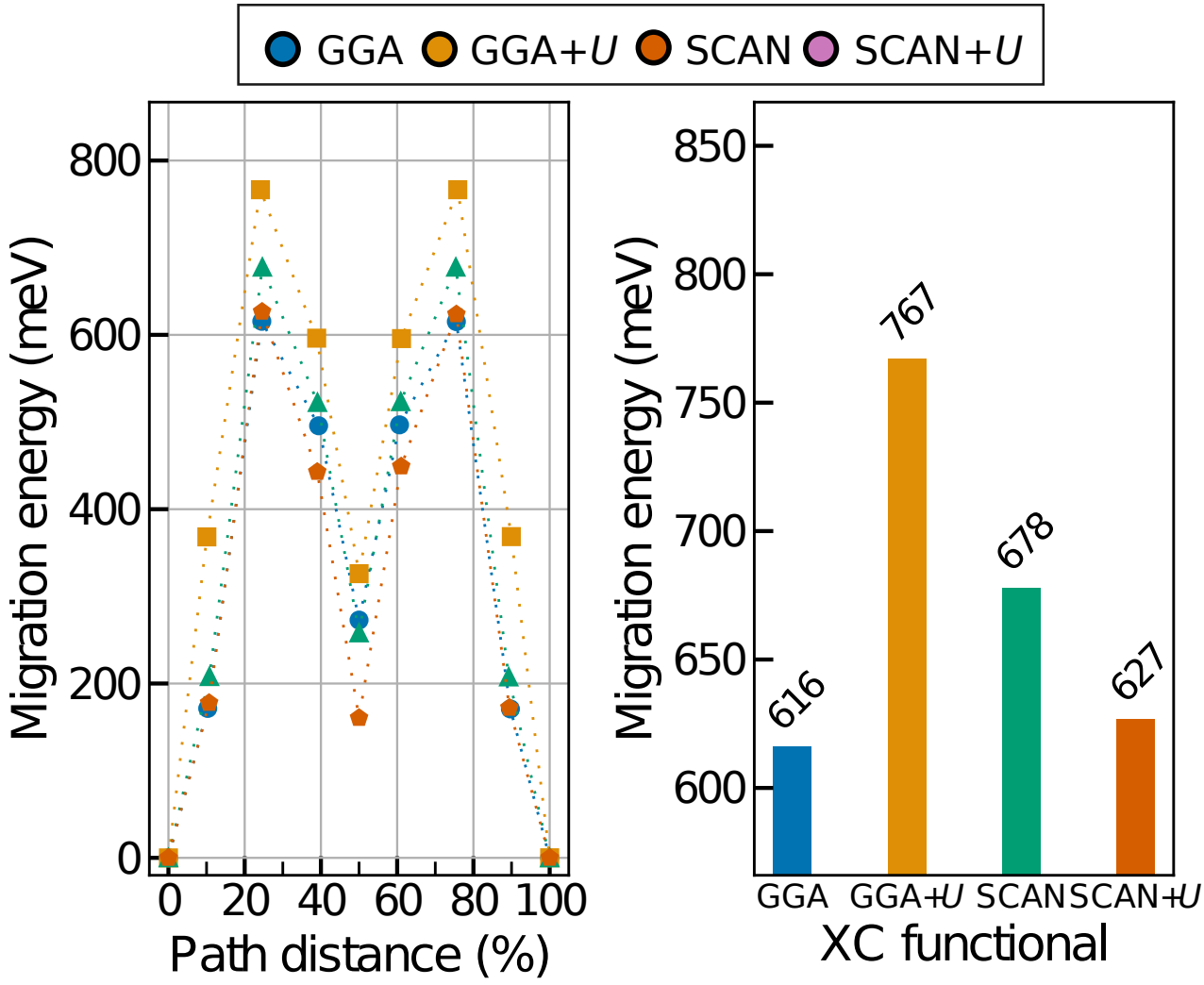

Supplementary Figure 6. MEPs and E_m for $Mg_xTi_2S_4$ for x = 0.148, i.e., the dilute Mg limit.

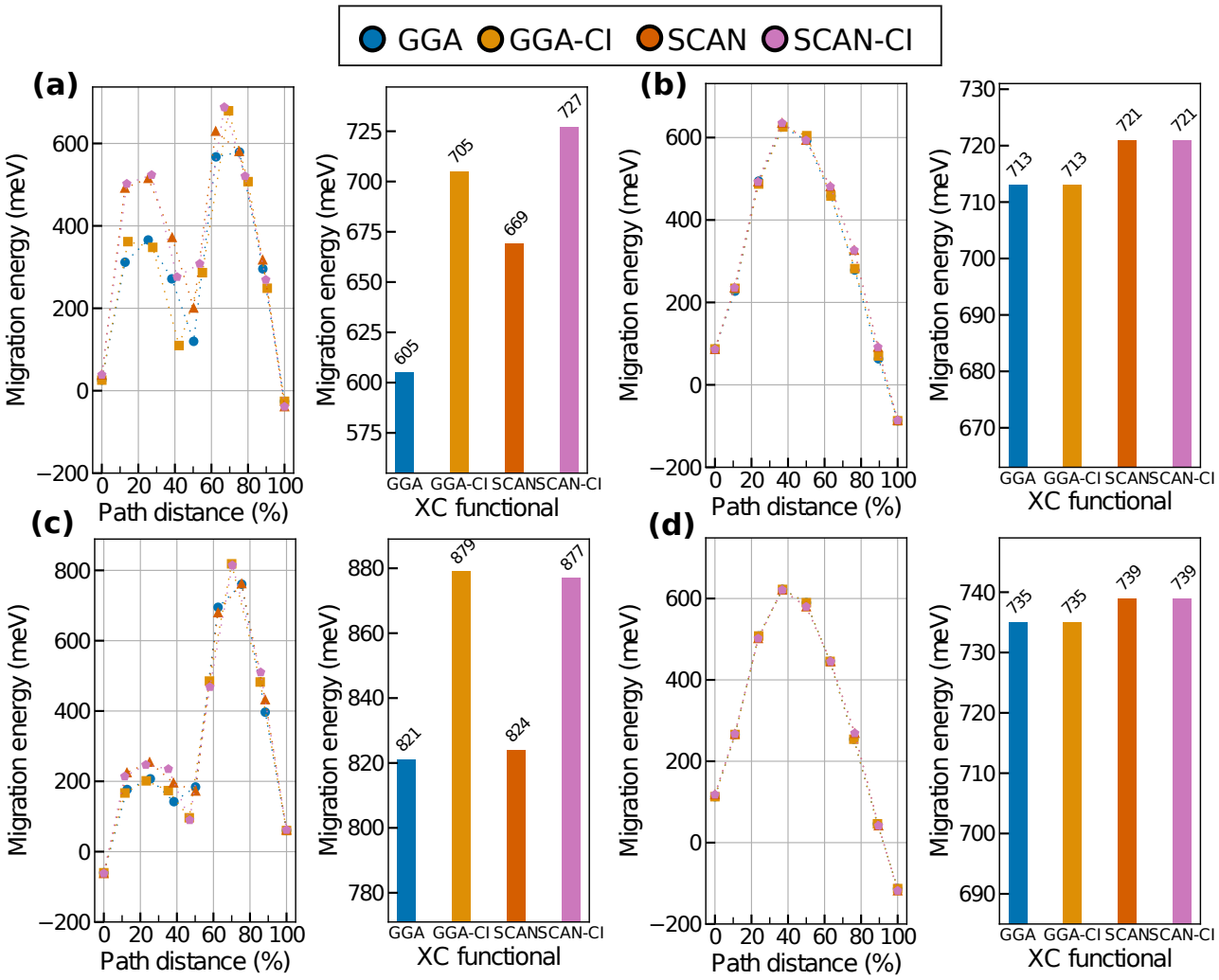

Supplementary Figure 7. MEPs and E_m for Li_3PO_4. Panels (a) and (b) correspond to the 1(d)→2(c)→3(d) hop and 2(c)→3(d) hop, respectively, without the inclusion of NELECT. Panels (c) and (d) are the same hops as in panels (a) and (b) but MEPs and E_m are calculated including NELECT.

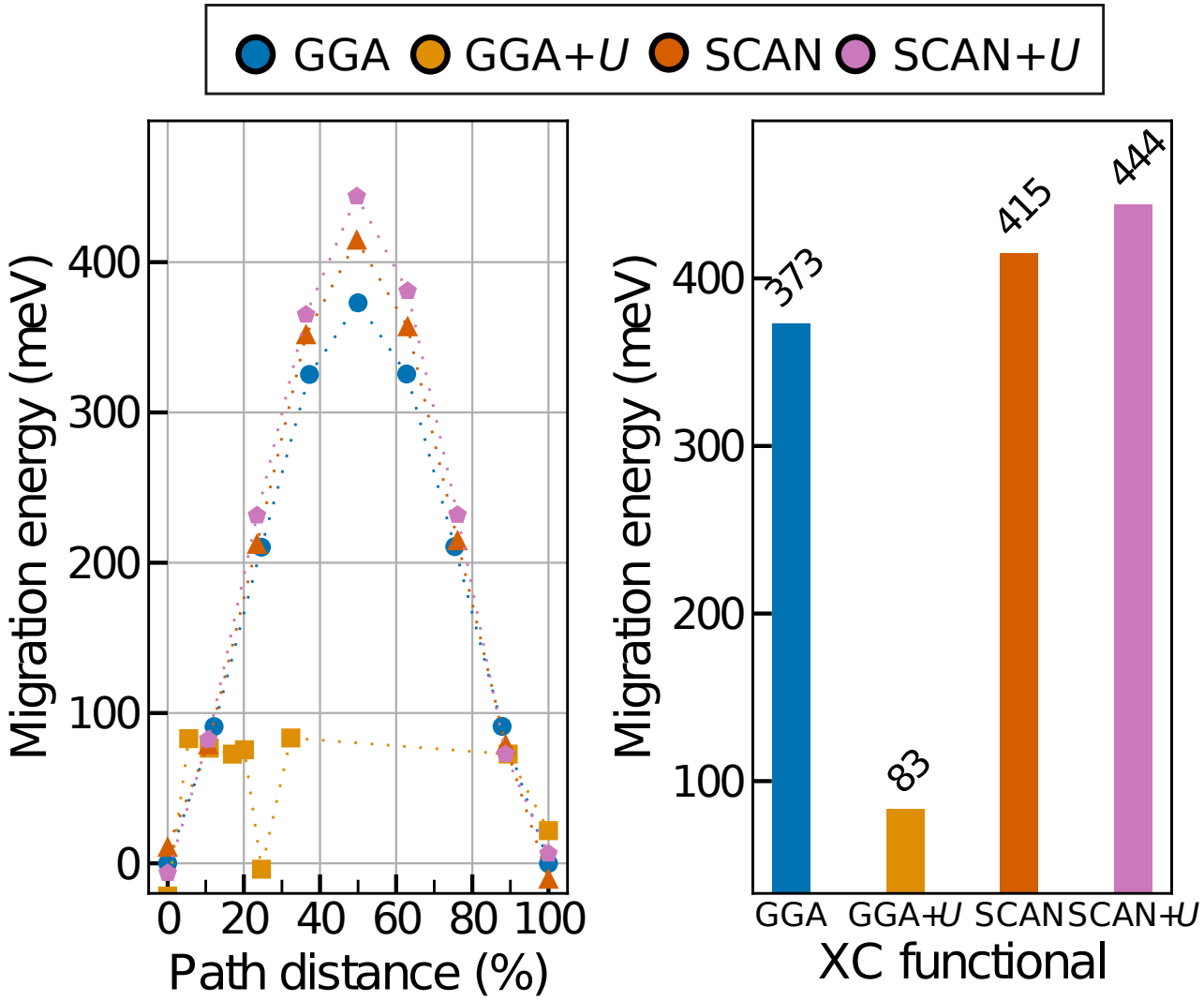

Supplementary Figure 8. MEPs and E_m for NaV_2O_4. The SCAN+*U* barrier was obtained from from a single-SCF calculation from converged SCAN-NEB geometries.

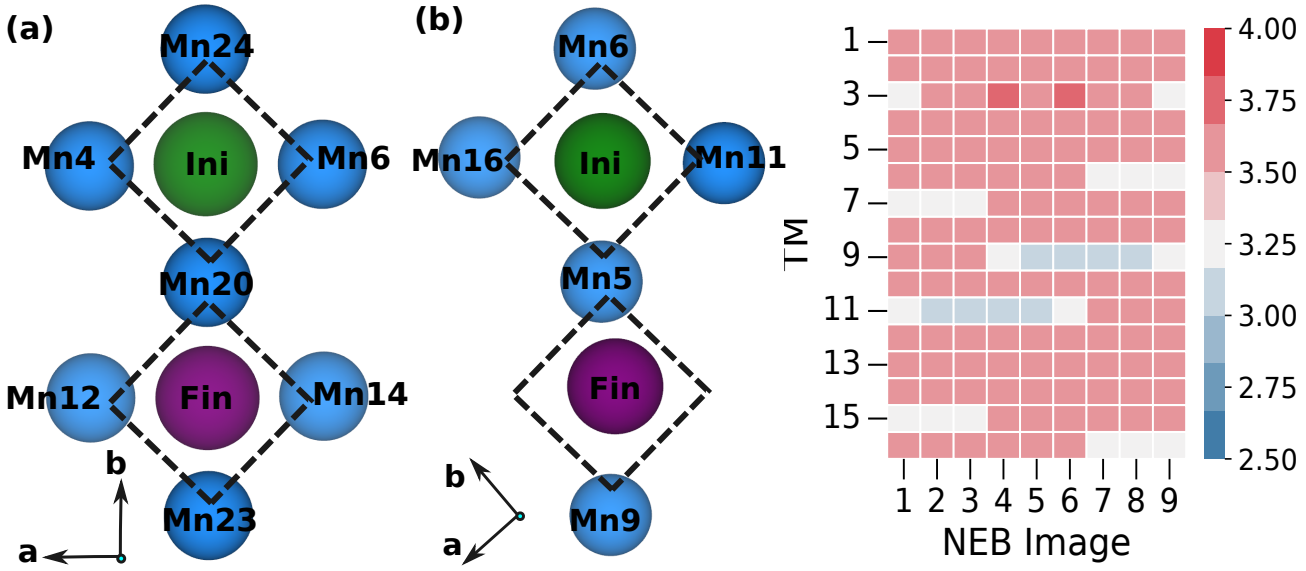

Supplementary Figure 9. (a) The position of the Mn relative to the initial (green circle) and the final (purple circle) Mg positions in $MgMn_2O_4$ in all NEB calculations, except GGA. (b) Mn positions and the on-site magnetic moments as a function of the image number in the GGA-NEB calculation. 'Ini' and 'Fin' indicate the initial and final positions of Mg during its migration.

References

1. Nakamura, K. *et al.* On the Diffusion of Li^+ Defects in $LiCoO_2$ and $LiNiO_2$. *Solid State Ion.* **135**, 143–147 (2000).
2. Verhoeven, V. W. J. *et al.* Lithium Dynamics in $LiMn_2O_4$ Probed Directly by Two-Dimensional Li NMR. *Phys. Rev. Lett.* **86**, 4314 (2001).
3. Schmidt, J. P. *et al.* Studies on $LiFePO_4$ as Cathode Material Using Impedance Spectroscopy. *J. Power Sources* **196**, 5342–5348 (2011).
4. Månsson, M. *et al.* Na-Ion Dynamics in Quasi-1D Compound NaV_2O_4. *J. Phys.: Conf. Ser.* **551**, 012035 (2014).
5. Bayliss, R. D. *et al.* Probing Mg Migration in Spinel Oxides. *Chem. Mater.* **32**, 663–670 (2019).
6. Sun, X. *et al.* A High Capacity Thiospinel Cathode for Mg Batteries. *Energy Environ. Sci.* **9**, 2273–2277 (2016).
7. Canepa, P. *et al.* High Magnesium Mobility in Ternary Spinel Chalcogenides. *Nat. Commun* **8**, 1–8 (2017).
8. Moon, C. K. *et al.* Vacancy-Driven Na^+ Superionic Conduction in New Ca-doped Na_3PS_4 for All-Solid-State Na-ion Batteries. *ACS Energy Lett.* **3**, 2504–2512 (2018).
9. Asai, T. & Kawai, S. NMR study of Li^+-ion diffusion in the solid solution $Li_{3+x}(P_{1-x}, Si_x)O_4$ with the γ_{II}-Li_3PO_4 structure. *Solid State Ion.* **7**, 43–47 (1982).